Supporting Information

Grason and Davidovitch 10.1073/pnas.1301695110

SI Text

1. Continuum Theory of Dislocation Scars

Energies. To study stable multidislocation patterns of confined sheets, we construct a continuum theory of neutral dislocation scars that decorate the sheet near its compressed boundary. [Note that hexagonal crystals of circular shape have (at least) six sites with fewer than four neighbors on their boundary. Such features, along with any "boundary defects" associated with cutting a circular boundary through the crystal, however, are completely screened by the boundary and generate no elastic stresses (similar to electrostatic charge on the surface of a conductor).] As explained in the main text, neutral scars take the form of linear chains of dislocations extending a distance ℓ_{sc} along the radial direction of the sheet from the free edge. For a weakly confined sheet in which the zone of compression is small ($\Delta\alpha \ll 1$), dislocations remain within a narrow strip near the free boundary, $\ell_{sc} \ll W$. In this limit, the curvature of the sheet edge is small on the scale of ℓ_{sc}, and we may treat the boundary region of the sheet as an infinite, half-space located at $y \geq 0$, where the boundary edge extends infinitely along the $\hat{x}$ direction, which is parallel to the Burgers vector $\mathbf{b}$ of stable dislocations. Thus, the Euclidean (x,y) coordinate system approximates the original polar coordinate system (r,θ) over a narrow radial band near the sheet edge ($r \to W - y$, $x \to W\theta$). To compute elastic energies of dislocations, we treat a dislocation as a "dipole" of disclination sources for stress (aligned along $\hat{y}$) subject to vanishing normal stress at $y = 0$, a boundary condition that requires "image" defects at positions reflected through the boundary at $y = 0$. The self-energy of a dislocation at distance y from the free boundary is (1)

$$E^d_{\rm self}(\mathbf{x}) = \frac{Yb^2}{8\pi}\left(1 + \ln\left[\frac{2y}{a}\right] + E_c\right), \qquad \text{[S1]}$$

where Y is the 2D Young modulus of the sheet, $a \approx b$ is the dipolar separation of 5–7 disclination pair, and $Yb^2E_c/(8\pi)$ is a microscopic "core energy" of the dislocation. It is convenient to write elastic interaction energy between dislocations at $\mathbf{x}_1$ and $\mathbf{x}_2$ as

$$E^d_{\rm int}(\mathbf{x}_1,\mathbf{x}_2) = \frac{Yb^2}{4\pi} + \frac{Yb^2}{8\pi}\partial_{y_1}\partial_{y_2}V(\mathbf{x}_1,\mathbf{x}_2), \qquad \text{[S2]}$$

where $V(\mathbf{x}_1,\mathbf{x}_2)$ describes long-range elastic interactions between disclinations,

$$V(\mathbf{x}_1,\mathbf{x}_2) = |\mathbf{x}_1 - \mathbf{x}_2|^2 \ln\left(\frac{|\mathbf{x}_1 - \mathbf{x}_2|}{|\mathbf{x}_1 - \bar{\mathbf{x}}_2|}\right). \qquad \text{[S3]}$$

Here, $\bar{x} = (x, -y)$ is the location of an image of the defect at $\mathbf{x}$, which is situated at a reflected position of the defect through the boundary at $y = 0$ (note that $|\mathbf{x}_1 - \bar{\mathbf{x}}_2| = |\bar{\mathbf{x}}_1 - \mathbf{x}_2|$).

Our analysis determines the number $n_{\rm sc}$ and length $\ell_{\rm sc}$ of scars, and the number N of dislocations per scar, by minimizing $U_{\rm scars}$, Eq. **7**. The asymptotic analysis that enables the analytic evaluation of $U_{\rm scars}$ relies on the limit of weak confinement ($\Delta\alpha \ll 1$) and—more profoundly—on the continuum limit $b/W \ll 1$. [Although we assume $(W/R)^2 \approx \alpha^*\gamma/Y \ll 1$, i.e., small strains, the asymptotic analysis does not explicitly involve the small limit of this parameter. More precisely, we compute $U_{\rm scars}$ in two limits: $\lim_{W/R\to 0}\lim_{b/W\to 0}\lim_{\Delta\alpha\to 0}$ and $\lim_{W/R\to 0}\lim_{\Delta\alpha\to 0}\lim_{b/W\to 0}$.] The parameter range ($\Delta\alpha \ll 1, b/W \ll 1$) splits into two domains, each of which is characterized by distinct "dominant balance" of the triplet $\{U_{\rm relax}, U_{\rm self}, U_{\rm inter}\}$, when one energy becomes negligible compared with the other two. We summarize the details of this analysis in Table S1, listing the dominant balance in each domain and the asymptotic behavior of n_{sc}, ℓ_{sc}, and N. The primary interest of this study is on the continuum limit $b/W \to 0$ at a fixed $\Delta\alpha \ll 1$; hence, we focus below on the right column of Table S1.

The self-energy of a scar follows from summation of the dislocation self-energies and dislocation pair interactions along a given scar (located at, say, $x = 0$):

$$\begin{aligned} U_{\rm self} &= \sum_{i=1}^{N} E^d_{\rm self}(y_i) + \sum_{i=2}^{N}\sum_{j<i}^{N} E^d_{\rm int}(y_i,y_j) \\ &= \frac{Yb^2}{8\pi}\left(N^2 + N(E_c+1)\right) + \frac{Yb^2}{8\pi}\sum_{i=1}^{N}\ln\left[\frac{2y_i}{a}\right] \\ &\quad + \frac{Yb^2}{8\pi}\sum_{i=1}^{N}\sum_{j<i}^{N}\partial_{y_i}\partial_{y_j}V(y_i,y_j), \end{aligned} \qquad \text{[S4]}$$

where we label dislocation positions along the scar by $y_i = id$, where $d = \lambda_\parallel^{-1}$ is the dislocation spacing along the scar. To make progress, we assume the large-N limit and approximate the sums by integration along the scar length, so the first sum becomes

$$\sum_{i=1}^{N}\ln\left[\frac{2y_i}{a}\right] \simeq \lambda_\parallel \int_0^{\ell_{\rm sc}} dy\ \ln\left[\frac{2y}{a}\right] = N[\ln(2\ell_{\rm sc}/a) - 1], \qquad \text{[S5]}$$

where $\lambda_\parallel = N/\ell_{\rm sc}$. (We derive the energetics of scars by assuming $N \gg 1$, although the continuum theory ultimately predicts an optimal number of dislocations per scar of order unity. This affects only the numerical prefactors of the estimated energies and does not have any qualitative impact on our analysis.) Because of the singular nature of interactions for $y_i = y_j$, we must take the continuum limit of the double sum in Eq. **S4** carefully. We divide the scar length into N domains of width d extending over $id - d/2 < y_i < id + d/2$, and replace the value of the summand by the mean value along that interval:

$$\partial_{y_i}\partial_{y_j}V(y_i,y_j)\big|_{y_j=jd} \simeq \lambda_\parallel \int_{jd-d/2}^{jd+d/2} d\tilde{y}_j\,\partial_{y_i}\partial_{\tilde{y}_j}V(y_i,\tilde{y}_j). \qquad \text{[S6]}$$

Making this substitution, and taking the upper limit of the first y_j integral halfway between dislocation at y_i and $y_i - d$, we find

$$\begin{aligned} \sum_{i=1}^{N}\sum_{j<i}^{N}\partial_{y_i}\partial_{y_j}V(y_i,y_j) &\simeq \lambda_\parallel^2\int_0^{\ell_{\rm sc}} dy_i \int_0^{y_i - d/2} dy_j\,\partial_{y_i}\partial_{y_j}V(y_i,y_j) \\ &= \lambda_\parallel^2\int_0^{\ell_{\rm sc}} dy_i\left[\partial_{y_i}V(y_i,y_j)\right]\Big|_{y_j=0}^{y_j=y_i-d/2} \\ &= \lambda_\parallel\int_0^{\ell_{\rm sc}} dy_i\left[\ln\left(\frac{d}{4y_i}\right) + \frac{1}{2}\right] \\ &= N\ln\left(\frac{d}{4\ell_{\rm sc}}\right) - \frac{N}{2}, \end{aligned} \qquad \text{[S7]}$$

where we have taken the lower limits of both integrals to $y = 0$, introducing negligible corrections to the assumed large N limit.

Combining the results of Eqs. **S5** and **S7** in Eq. **S4** and multiplying by the total scar number, we arrive at the form of scar self-energy $U_{\rm self}$ of Eq. **10**.

Let us now consider the relative size of $U_{\rm self}$ and $U_{\rm relax}$, Eqs. **10** and **9**, respectively. Both energies represent additive scar energies and thus are linear in $n_{\rm sc}$, but the cost $U_{\rm self}$ is quadratic in N and b whereas the gain $U_{\rm relax}$ is linear in Nb and quadratic in $\ell_{\rm sc}$. Because the minimal dislocation number is $N=1$ and the maximal scar length is $\ell_{\rm sc}=3\ell_{\rm axi}\sim\Delta\alpha$, we conclude that $U_{\rm self}\gg|U_{\rm relax}|$ in the asymptotic domain $(\Delta\alpha)^2\ll b/W\ll 1$. Because both $U_{\rm self}$ and $U_{\rm inter}$ are positive costs, we obtain that $U_{\rm scars}>U_{\rm axi}$ in that domain, implying that the axisymmetric state is stable to scars if the compression level is sufficiently small. Turning now to the complementary domain, $b/W\ll(\Delta\alpha)^2\ll 1$, the above considerations imply $U_{\rm self}\ll|U_{\rm relax}|$, and we conclude that the dominant balance in the triplet $\{U_{\rm self},U_{\rm inter},U_{\rm relax}\}$ consists of the last two terms.

Let us now compute $U_{\rm inter}$, recalling that it must satisfy $U_{\rm inter}\gg U_{\rm self}$. We express $U_{\rm inter}$ as a sum over scar–scar interaction energies, $E_{\rm inter}(x)$, the elastic interaction between scars separated by a distance x along the edge. Evaluating the sum over dislocation pair interactions follows a method similar to that of the self-energy of scars:

$$\begin{aligned}E_{\rm inter}(x)&=\frac{Yb^2\lambda_{\|}^2}{8\pi}\int_0^{\ell_{\rm sc}}dy\int_0^{\ell_{\rm sc}}dy'\left[1+\partial_y\partial_{y'}V(\mathrm{x},\mathrm{x}')\right]\\&=\frac{Yb^2N^2}{4\pi}\left[1+\frac{x^2}{4\ell_{\rm sc}^2}\ln\left(\frac{x^2}{x^2+4\ell_{\rm sc}^2}\right)\right].\end{aligned}\qquad\textbf{[S8]}$$

Comparing now the energies $U_{\rm self}$ and $U_{\rm inter}$, we obtain the relation $U_{\rm inter}\sim(n_{\rm sc}\ell_{\rm sc}/W)U_{\rm self}$. The geometric meaning of this relation is depicted in Fig. 1*D*, which shows that scars interact strongly within a lateral distance or order $\ell_{\rm sc}$. Because the above asymptotic analysis (right column of Table S1) implies $U_{\rm inter}\gg U_{\rm self}$, we find that the continuum limit of weak compression, $b/W\ll(\Delta\alpha)^2\ll 1$, is characterized by a dense distribution of scars: $n_{\rm sc}\gg 1/\Delta\alpha$. This proves the asymptotic relation noted in Eq. **8**. A more systematic proof of this relation requires evaluation of $U_{\rm inter}$ as the sum over $E_{\rm inter}(x)$ in the two limits: (*a*) "dilute" scars: $x\gg 2\ell_{\rm sc}$, where we find that scar interactions fall to zero at $E_{\rm inter}\sim 1/x^2$, and the resulting $U_{\rm inter}\ll U_{\rm self}$, in contradiction to the asymptotic requirement $U_{\rm inter}\gg U_{\rm self}$, and (*b*) "dense" scars: $x\ll 2\ell_{\rm sc}$. In this limit, integrating $E_{\rm inter}(x)$ over a linear edge density of scars $n_{\rm sc}/(2\pi W)$ and multiplying by the scar number leads to the form of scar interaction energy $U_{\rm inter}$ of Eq. **11**, which satisfies $U_{\rm inter}\gg U_{\rm self}$ as required.

Stress Collapse. In this section, we briefly derive the stress profile near the edge of a weakly confined sheet in the presence of an array of $n_{\rm sc}$ scars of length $\ell_{\rm sc}$ composed of N dislocations, assuming again that scars remain sufficiently close to the free boundary that we may approximate the sheet geometry as an infinite half-space ($y<0$). The total stress derives from the superposition of the stress in the axisymmetric state and the dislocation-induced stress, $\sigma^{\rm scars}=\sigma^{\rm axi}+\sigma^{\rm dis}$. We compute $\sigma^{\rm dis}$ in the continuum limit where we neglect fine scale variations of dislocation density within the scarred domain, approximating the distribution as a uniform areal density of dislocations $\rho_0=n_{\rm sc}N/(2\pi W\ell_{\rm sc})$ within the region $y<\ell$. In addition to the conditions of force balance, the stress is governed by the compatibility condition (2) modified by the distribution of dislocations $\rho(y)=\rho_0\theta(\ell-y)$,

$$Y^{-1}\nabla^2\left(\sigma_{xx}^{\rm dis}+\sigma_{yy}^{\rm dis}\right)=-b\partial_y\rho(y).\qquad\textbf{[S9]}$$

In the continuum approximation, dislocation stress is uniform along the edge direction and $\sigma_{xy}^{\rm dis}=0$, so the equations of force balance reduce to

$$\partial_y\sigma_{yy}^{\rm dis}=0.\qquad\textbf{[S10]}$$

Boundary conditions require that $\sigma_{yy}^{\rm dis}(y=0)=0$; hence, Eq. **S10** implies $\sigma_{yy}^{\rm dis}=0$. From Eq. **S9**, the discontinuity of dislocation density at the edge of the scar zone requires discontinuous derivatives of the edge stress,

$$\partial_y\sigma_{xx}^{\rm dis}\big|_{y>\ell_{\rm sc}}-\partial_y\sigma_{xx}^{\rm dis}\big|_{y<\ell_{\rm sc}}=Yb\rho_0.\qquad\textbf{[S11]}$$

Because the dislocation stress vanishes far from the boundary (as $y\to\infty$), $\partial_y\sigma_{xx}^{\rm dis}|_{y>\ell_{\rm sc}}=\sigma_{xx}^{\rm dis}(y>\ell_{\rm sc})=0$. The edge (or hoop) component of dislocation-induced stress for the multiscar geometry then has the form

$$\sigma_{xx}^{\rm dis}=\begin{cases}Yb\rho_0(\ell_{\rm sc}-y) & y<\ell_{\rm sc}\\ 0 & y>\ell_{\rm sc}\end{cases}.\qquad\textbf{[S12]}$$

For minimal energy scars, dislocation-induced stress perfectly cancels the edge (hoop) component of $\sigma^{\rm axi}$ within the zone of compression $y<\ell_{\rm axi}$. To see this, we can take $\ell_{\rm sc}=\ell_{\rm axi}$ and $\rho_0=b^{-1}(Y/\gamma)(\Delta\alpha)/\ell_{\rm axi}$, which follows from the "slaving condition" of Eq. **12**. Comparing Eq. **S12** with the axisymmetric stress of Eq. **5**, we see that $\sigma_{xx}^{\rm dis}(y<\ell_{\rm axi})=-\sigma_{xx}^{\rm axi}(y<\ell_{\rm axi})$, resulting in collapse of the compressive stress, $\sigma_{xx}^{\rm scar}(y<\ell_{\rm axi})=0$.

2. Compression-Free Stress Field: Spherical Substrate

The compression-free stress field must satisfy $\sigma_{ii}\geq 0$, where i labels the two principle directions of the stress tensor. This type of stress field was first studied as the "membrane limit" of wrinkle patterns in very thin sheets (3–6). For axisymmetrically stretched sheets, such as the one addressed in the current study, the two principle directions are everywhere $\hat r,\hat\theta$ and the compression-free stress field is characterized naturally by a two-zones structure, similar to the stress of the axisymmetric state, Eq. **2**: (*i*) an inner zone $(0<r<L)$, where both radial and hoop stresses are tensile: $\sigma_{rr}>0,\sigma_{\theta\theta}>0$, and (*ii*) an outer annulus $(L<r<W)$, where the radial stress is tensile and the hoop stress vanishes. (The shear stress $\sigma_{r\theta}$ vanishes in both zones.) The value of L is found by matching the stress between the two zones. (Details of this procedure may be found in ref. 6, which addresses the planar stretching of an annulus under radial tension gradient.)

- In the inner zone, where the stress is purely tensile, the sheet is at an axisymmetric state; hence, the stress field there may be obtained from $\sigma^{\rm axi}(r;\alpha)$ (Eq. **2**) by replacing

$$W\to L;\ \gamma\to\sigma_{rr}(L);\ \alpha\to\overline{\alpha}=[Y/\sigma_{rr}(L)]\cdot(L/R)^2,\qquad\textbf{[S13]}$$

where $L,\sigma_{rr}(L)$ are two unknowns (to be found below). Hence,

$$(0<r<L):\ \sigma_{\theta\theta}(r)/\sigma_{\rm rr}(L)=\overline{\alpha}\left[1-3(r/L)^2\right]\Big/16+1\qquad\textbf{[S14a]}$$

$$(0<r<L):\ \sigma_{rr}(r)/\sigma_{rr}(L)=\overline{\alpha}\left[1-(r/L)^2\right]\Big/16+1.\qquad\textbf{[S14b]}$$

- In the outer annulus, $L<r<W$, where $\sigma_{r\theta}=\sigma_{\theta\theta}=0$, the force balance in the radial direction $\hat r$ becomes $\partial_r(r\sigma_{rr})=0$, and using the boundary condition $\sigma_{rr}(r=W)=\gamma$, we obtain

$$(L<r<W):\ \sigma_{rr}=\gamma W/r;\ \sigma_{\theta\theta}=0.\qquad\textbf{[S15]}$$

- The length L and the stress $\sigma_{rr}(L)$ are determined by requiring both stress components $\sigma_{rr}, \sigma_{\theta\theta}$ to be continuous at the borderline $r=L$ between the two zones, namely as $r\to L^+$ and $r\to L^-$. Continuity of $\sigma_{\theta\theta}$ implies that $\sigma_{\theta\theta}(r)$ in the axisymmetric zone $(r\le L)$ approaches zero at $r=L$, and therefore the effective confinement parameter $\overline{\alpha}$ in Eq. **S13** must equal the critical confinement value $\alpha^*=8$ at which compression emerges. Thus, the continuity of the radial and hoop stresses yields two equations for L and $\sigma_{rr}(L)$:

$$\sigma_{rr}(L)=\gamma W/L \qquad \textbf{[S16]}$$

$$\overline{\alpha}=\frac{Y}{\sigma_{rr}(L)}\left(\frac{L}{R}\right)^2=\alpha\left(\frac{L}{W}\right)^3=\alpha^*. \qquad \textbf{[S17]}$$

Hence we obtain the radius of the unwrinkled region:

$$L=W\left(\frac{\alpha^*}{\alpha}\right)^{1/3}. \qquad \textbf{[S18]}$$

For the limit of weak confinement addressed in our study, we expand Eq. **S18** around α^* and find

$$L\approx W\left(1-\frac{1}{3}\Delta\alpha\right), \qquad \textbf{[S19]}$$

which is identical to $\ell_{\rm axi}$ (Eq. **4**).

3. Wrinkle Pattern

The nature of the subdominant wrinkle energy is elucidated by first considering the force balance in the normal direction to the sheet. For our study, in which the slope $\sim W/R\ll 1$, we use the Föppl–von Kármán (FvK) framework, taking the two tangential directions to be the radial $\hat{\mathbf{r}}$ and azimuthal $\hat{\boldsymbol{\theta}}$ at the plane of the undeformed sheet; hence, the normal direction $\hat{\boldsymbol{n}}$ may be approximated by the perpendicular $\hat{\boldsymbol{z}}$ to that plane. The normal force balance (first FvK equation) becomes

$$\begin{aligned}B\Delta^2\zeta-\sigma_{rr}\partial_r^2\zeta-\frac{2}{r}\sigma_{r\theta}\left(\partial_r-\frac{1}{r}\right)\partial_\theta\zeta-\frac{1}{r^2}\sigma_{\theta\theta}\left(\partial_\theta^2\zeta+r\partial_r\zeta\right)\\=-K\left[\zeta(r,\theta)-\zeta_{sph}(r)\right],\end{aligned} \qquad \textbf{[S20]}$$

where the Laplacian $\Delta\equiv\partial_r^2+\frac{1}{r}\partial_r+\frac{1}{r^2}\partial_\theta^2$ and $\zeta_{sph}(r)\approx r^2/2R$ is the original state of the spherical substrate. (A Winkler foundation with $K\approx E_s/H$ characterizes a rigid sphere of radius R covered by a compliant layer of Young modulus E_s and thickness $H\ll R$. The local response of this model captures qualitatively the more complex, nonlocal response of homogenous solid substrates.) Consider now the wrinkle pattern,

$$\zeta(r,\theta)=\zeta_0(r)+f(r)\cos(m\theta), \qquad \textbf{[S21]}$$

which we address in the singular, high-bendability limit $(\epsilon_b\to 0)$, where $f(r)\to 0$ and $m\to\infty$ such that the product $mf(r)$ remains finite as $\epsilon_b\to 0$ (the slaving condition, Eq. **19**). Substituting this form in the force balance, Eq. **S20**, we obtain an equation for the oscillatory term $(\propto f\cos(m\theta))$ and an equation for the nonoscillatory one, which does not involve $f(r)$.

- The nonoscillatory equation is

$$B\left(\frac{d^2}{dr^2}+\frac{1}{r}\frac{d}{dr}\right)^2\zeta_0-\sigma_{rr}\frac{d^2}{dr^2}\zeta_0-\frac{1}{r}\sigma_{\theta\theta}\frac{d}{dr}\zeta_0=-K\left[\zeta_0-\zeta_{sph}(r)\right]. \qquad \textbf{[S22]}$$

In the high bendability regime $(\epsilon_b\ll 1)$, the force associated with radial bending $(\sim B\zeta_0''')$ is negligible with respect to the other forces. Furthermore, for sufficiently rigid substrates, Eq. **S22** simply forces negligible deviation of the radial profile $\zeta_0(r)$ from the original spherical shape of the substrate, $\zeta_0\approx\zeta_{sph}(r)$, and the corresponding components of the stress field $\sigma_{rr}(r)$, $\sigma_{\theta\theta}(r)$ then are given by the compression-free form described above, Eqs. **S14**, **S15**, and **S18**). [Dimensional analysis, to be presented elsewhere, shows that the low-deformability regime, where $\zeta_0(r)\approx\zeta_{sph}(r)$ correspond to $\tilde{K}=KR^2/Y\gg 1$, thus limiting the current analysis to the parts painted in solid colors in Fig. 2 of the main text.]

- The oscillatory part of Eq. **S20** takes a simplified form in the high-bendability regime, where $|\partial_\theta\zeta|\sim|mf(r)|\gg|df/dr|$, and the radial stress $\sigma_{rr}\approx\gamma W/r$ (Eq. **S15**). Thus, we obtain the equation

$$B\frac{m^4}{r^4}f-\sigma_{rr}\frac{d^2f}{dr^2}+Kf=-\frac{m^2}{r^2}\sigma_{\theta\theta}f, \qquad \textbf{[S23]}$$

where the right-hand side is the destabilizing force and the left-hand side consists of the three relevant restoring forces, associated with the bending rigidity of the sheet, tension in the radial direction, and stiffness of the spherical substrate. The energetic costs associated with these restoring forces, are, respectively,

$$\frac{1}{4}\int_L^W rdr\, B\frac{m^4f^2}{r^4}\Rightarrow U_{\rm bend}\sim YW^2\epsilon_b\left(\frac{\gamma}{Y}\right)^2(\Delta\alpha)^2m^2, \qquad \textbf{[S24a]}$$

$$\frac{1}{4}\int_L^W rdr\,\sigma_{rr}\left(\frac{df}{dr}\right)^2\Rightarrow U_{\rm tens}\sim YW^2\left(\frac{\gamma}{Y}\right)^2m^{-2}, \qquad \textbf{[S24b]}$$

$$\frac{1}{4}\int_L^W rdr\,Kf^2\Rightarrow U_{\rm subst}\sim YW^2\tilde{K}\left(\frac{\gamma}{Y}\right)^2(\Delta\alpha)^2m^{-2}, \qquad \textbf{[S24c]}$$

where we used the slaving condition, Eq. **19**, together with the estimated area of the wrinkled zone $(\int_L^W rdr\sim W^2\Delta\alpha)$ and the estimated radial derivative $|df/dr|\sim f/\ell\sim f/W\Delta\alpha$ to express the energies as single-variable functions of the wrinkle number m.

As was noted already by Cerda and Mahadevan (7), the fact that $U_{\rm subst}$ and $U_{\rm tens}$ scale similarly with the wrinkle number $(\sim m^{-2})$ implies that the subdominant wrinkle energy $U_{\rm wrink}^{\rm sub}$ is governed by a balance of $U_{\rm bend}$ and $\max\{U_{\rm tens},U_{\rm subst}\}$, such that the wrinkle number m that minimizes $U_{\rm wrink}^{\rm sub}$ may be expressed as

$$m\sim W\left(K_{\rm eff}/B\right)^{1/4};\ K_{\rm eff}=\max\left\{K,\gamma/(W\Delta\alpha)^2\right\}. \qquad \textbf{[S25]}$$

The parameter $K_{\rm eff}$ is the effective stiffness of a supported, uniaxially stretched sheet to the formation of wrinkles of length $\ell\sim W(\Delta\alpha)$ (7).

Implementing this principle for our problem (using the above estimates in Eq. **S24**), we find that the subdominant wrinkle energy $U_{\rm wrink}^{\rm sub}$ and the number of wrinkles m can be conveniently expressed by defining the bendability and deformability parameters (Eqs. **21** and **22**), leading to the three characteristic parameter regimes, denoted W1–W3 in the text. [A more careful analysis of this regime yields corrections $\sim\log(\epsilon)$ to the number m and the energy $U_{\rm wrink}^{\rm sub}$ that may be ignored in the current analysis. Also, note that as $\Delta\alpha\to\epsilon^{1/4}$, Eq. **24** implies $m\sim\epsilon^{-3/8}$, in accord with the near-threshold analysis (6).] We reemphasize that this wrinkling analysis applies to the asymptotic parameter range $(\epsilon\ll 1,\tilde{K}\gg 1,\Delta\alpha\ll 1)$, which corresponds to very thin sheets

(because $B \sim t^3$) or large radial tension, a stiff substrate, and weak confinement. [For $\tilde{K} < 1$, the spherical substrate flattens beneath the sheet (17), invalidating our calculations of the axisymmetric energy U_{axi} and the dominant energy U^{dom} of the compression-free stress.]

4. Hyperbolic Substrate

In this section, we briefly analyze the axisymmetric and compression-free stress fields for the circular sheets confined to a hyperbolic surface of constant negative Gaussian curvature, $G = -R^{-2}$. As in the case of the sheet on the spherical substrate, we consider the case of a finite radial tension at the boundary of the sheet $\sigma_{rr}(r = W) = \gamma > 0$. In contrast to a spherical cap ($G = R^{-2}$), the saddle's shape is not axisymmetric. Nevertheless, as long as the Gaussian curvature is axisymmetric (as is the case for a constant G), the stress field has axisymmetric solutions, which do not involve shear, and we expect both wrinkled (scarred) and unwrinkled (unscarred) states of the sheet to be described by such stress fields. We first will describe the stress field of the featureless state (unwrinkled, unscarred), which is the analog of the compressed, axisymmetric state of the spherical cap (Fig. 1*E*), and then we will discuss the collapse of stress by the formation of wrinkles or scars.

Unwrinkled, Unscarred State. Considering the analogous state of the axisymmetric state of a sheet on a spherical cap (Eq. **2**), we note that the sign inversion of substrate curvature affects a sign inversion (compression ↔ tension) of the "geometric" part of the stress profile (the part that is proportional to r^2). Thus, we find

$$\begin{aligned}\sigma_{\theta\theta}^{\text{axi}}(r)/\gamma &= -\alpha\left[1 - 3(r/W)^2\right]\Big/16 + 1\\ \sigma_{rr}^{\text{axi}}(r)/\gamma &= -\alpha\left[1 - (r/W)^2\right]\Big/16 + 1,\end{aligned} \qquad \textbf{[S26]}$$

where we retain the same definition of confinement $\alpha = (W/R)^2(Y/\gamma)$. Unlike the positive curvature case, both radial and hoop components of stress have regions of tension and compression (Fig. 1*G*). For negatively curved substrates, there is a critical confinement, $\alpha^* = 16$, below which compression is eliminated from the axisymmetric state [namely, for sufficiently large radial tension at the edge, $\sigma_{rr}(W) = \gamma > YW^2/16R^2$, both radial and hoop directions are under tension everywhere in the sheet]. For $\alpha > \alpha^*$, there are three zones determined by the radial scales:

$$L_\theta^{\text{axi}}(\alpha) = W\frac{1}{\sqrt{3}}(1 - \alpha^*/\alpha)^{1/2};\; L_r^{\text{axi}}(\alpha) = W(1 - \alpha^*/\alpha)^{1/2}, \qquad \textbf{[S27]}$$

which describe, respectively, points of vanishing hoop and radial stress:

i) $r < L_\theta^{\text{axi}}$, for which $\sigma_{\theta\theta}^{\text{axi}} < 0$ and $\sigma_{rr}^{\text{axi}} < 0$;

ii) $L_\theta^{\text{axi}} < r < L_r^{\text{axi}}$, for which $\sigma_{\theta\theta}^{\text{axi}} > 0$ and $\sigma_{rr}^{\text{axi}} < 0$;

iii) $r > L_r$, for which $\sigma_{\theta\theta}^{\text{axi}} > 0$ and $\sigma_{rr}^{\text{axi}} > 0$.

Collapse of Hoop Stress. In analogy to section 2, we expect that the stress field of the wrinkled or scarred state (in the respective high-bendability or defectability regime) consists of two zones: an outer zone at $L < r < W$, where the radial stress is tensile ($\sigma_{rr} > 0$) such that the boundary condition $\sigma_{rr}(W) = \gamma$ is satisfied, and an inner zone $0 < r < L$. We now consider the possibilities by which such a stress field (enabled by wrinkles or scars) can lower the high energetic cost of Eq. **S26**.

- Assume first that hoop tension $\sigma_{\theta\theta}$ is relaxed by scars that develop in the outer zone, such that the stress field is characterized by a profile similar to that of Eq. **S15**, where the only nonvanishing stress component is the radial tension σ_{rr}. Again, radial force balance and the boundary condition $\sigma_{rr}(W) = \gamma$ give rise to radial tension $\sigma_{rr}(r) = \gamma W/r$, which increases with the distance from the edge of the sheet. Obviously, such a radial stress profile, which is implied by assuming a compression-free zone (where $\sigma_{\theta\theta} = 0$) cannot exist in the whole sheet because of the divergence $\sigma_{rr} \sim r^{-1}$ as $r \to 0$. Hence, there must be an inner zone ($r < L$ for some $0 < L < W$) where $\sigma_{\theta\theta}$ does not vanish. Radial force balance at $r = L$ requires $\sigma_{rr}(L) = \gamma W/L$; hence, the radial stress cannot collapse at the inner zone. Hence (similar to section 2), the stress in the inner zone is described by Eq. **S26** under the substitution $W \to L$; $\gamma \to \gamma W/L$. The resulting stress, for some value of $0 < L < W$, is plotted in Fig. S1. Simply put, for any finite radial tension at the boundary, there is no solution that collapses hoop tension everywhere in the sheet. The actual value of L must be determined here by minimizing the dominant energy over all possible values of $0 < L < W$, similarly to ref. 6. This minimization procedure involves some subtleties (in comparison with ref. 6, where L marks a compression-free rather than tension-free zone), and we will not discuss it further here. We note, however, that comparison between the profiles in Fig. S1 and Fig. 1*H* indicates a higher level of stress in the hoop tension-free stress in comparison with the compression-free stress (which we discuss below). It thus is plausible to expect that collapse of hoop tension is not the favorable energetic mechanism to relax stress in a stretched sheet on a saddle.
- Next, we consider the collapse of hoop stress for the negatively curved saddle substrate within an inner annulus $r < L$ in the sheet (shown in Fig. 1*H*). Because radial force balance requires $r\sigma_{rr}$ to be constant when $\sigma_{\theta\theta} = 0$, finite stress at $r \to 0$ also requires radial stress to vanish

$$(r < L):\; \sigma_{rr} = \sigma_{\theta\theta} = 0. \qquad \textbf{[S28]}$$

In the outer region, boundary conditions and axisymmetry require that the stress be described by Eq. **S26**

$$(L \le r < W):\; \sigma_{rr} = \sigma_{rr}^{\text{axi}};\; \sigma_{\theta\theta} = \sigma_{\theta\theta}^{\text{axi}}. \qquad \textbf{[S29]}$$

Matching the radial stress at the boundary between the two regions $\sigma_{rr}(r = L_-) = \sigma_{rr}(r = L_+)$, we find that

$$L(\alpha)/W = L_r^{\text{axi}}(\alpha)/W = (1 - \alpha^*/\alpha)^{1/2}. \qquad \textbf{[S30]}$$

We find that for the negative-curvature saddle substrate, the compression-free zone extends beyond the region of the hoop compression of the unwrinkled, unscarred state, to the same size as the zone of radial compression. We note the unusual appearance of a discontinuity in $\sigma_{\theta\theta}$ at $r = L$. Such a discontinuity will give rise to a "boundary layer" that smooths the singular feature and contributes to the subdominant costs of wrinkle or scar patterns (see ref. 9 for the behavior of a conceptually similar boundary layer at the end of the wrinkled zone in a stretched sheet).

Other Negatively Curved Substrates. We chose to study here the stretching of a sheet on a saddle-shaped substrate as an example of the class of hyperbolic (negatively curved) substrates. This choice is motivated by a recent theoretical study (10) and, importantly, by the intimate relation between the stress field of the sheet in this example and the stress field of a sheet on a spherical cap. Comparison between Fig. 1*H* and Fig. S1 suggests that under conditions of stretching at the boundary ($\sigma_{rr}(W) = \gamma > 0$), the sheet will tend to collapse hoop and radial compression away from the boundary, rather than collapse hoop tension near the boundary. This conclusion is in agreement with the observations

in ref. 10. It is important to note, however, that we do anticipate situations in which a collapse of tension (near or away from boundaries) is energetically favorable. In the context of a sheet on saddle, such a scenario may occur if the sheet in subjected to finite radial compression at the boundary (although it may be doubted whether such a system is stable against delamination of the sheet from the substrate). Attaching a sheet to other types of negatively curved substrates also may lead to the formation of a pattern in which tension collapses, such as the catenoidal interfaces studied in ref. 11.

1. Hirth JP, Lothe J (1982) *Theory of Dislocations* (Wiley, New York).
2. Nelson DR (2002) *Defects and Geometry in Condensed Matter Physics* (Cambridge Univ Press, Cambridge, UK).
3. Stein M, Hedgpeth JM (1961) *Analysis of Partly Wrinkled Membranes* (Natl Aeronautics Space Admin, Washington), Technical Note D-813.
4. Pipkin AC (1986) The relaxed energy density for isotropic elastic membranes. *IMA J Appl Math* 36:85–99.
5. Mansfield EH (1989) *The Bending and Stretching of Plates* (Cambridge Univ Press, Cambridge, UK).
6. Davidovitch B, Schroll RD, Vella D, Adda-Bedia M, Cerda EA (2011) Prototypical model for tensional wrinkling in thin sheets. *Proc Natl Acad Sci USA* 108(45):18227–18232.
7. Cerda E, Mahadevan L (2003) Geometry and physics of wrinkling. *Phys Rev Lett* 90(7):074302.
8. King H, Schroll RD, Davidovitch B, Menon N (2012) Elastic sheet on a liquid drop reveals wrinkling and crumpling as distinct symmetry-breaking instabilities. *Proc Natl Acad Sci USA* 109(25):9716–9720.
9. Davidovitch B, Schroll RD, Cerda E (2012) Nonperturbative model for wrinkling in highly bendable sheets. *Phys Rev E Stat Nonlin Soft Matter Phys* 85(6 Pt 2):066115.
10. Yao Z, Bowick M, Ma X, Sknepnek R (2013) Planar sheets meet negative-curvature interfaces. *Eur Phys Lett* 101:44007.
11. Irvine WTM, Vitelli V, Chaikin PM (2010) Pleats in crystals on curved surfaces. *Nature* 468(7326):947–951.

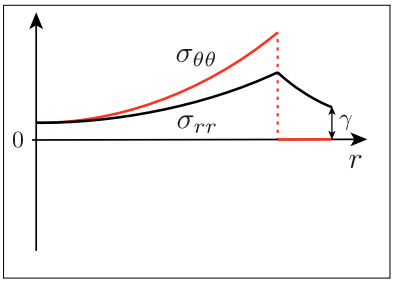

Fig. S1. Dominant stress pattern achievable by collapse of hoop stress $(\sigma_{\theta\theta} = 0)$ in an annular zone $L < r < W$ for a constant, negative-curvature substrate.

Table S1. Dominant balance and asymptotic limits

Parameter regime	$(\Delta\alpha)^2 \ll b/W \ll 1$ (no scars)	$b/W \ll (\Delta\alpha)^2 \ll 1$ (scars)
Energetic dominance	$U_{\text{self}} \sim U_{\text{inter}} \gg \lvert U_{\text{relax}}\rvert$	$\lvert U_{\text{relax}}\rvert \sim U_{\text{inter}} \gg U_{\text{self}}$
Energetic stability	$U_{\text{scars}} > U_{\text{axi}}$	$U_{\text{scars}} < U_{\text{axi}}$
ℓ_{sc}/W		$\rightarrow \Delta\alpha/3$
N		$\rightarrow$ *constant*
n_{sc}		$\sim (W/b)(\gamma/Y)$